Mechanism of Thiol Oxidation by the Superoxide Radical

Bruno Cardey, Sarah Foley, and Mironel Enescu*

University of Franche-Comte, Laboratoire de Microanalyses Nucleaires, UMR CEA E4, 16 route de Gray, 25030 Besancon, France

Received: April 23, 2007; In Final Form: October 3, 2007

In spite of the large quantity of experimental work that deals with the oxidation of thiols by superoxide, the mechanism of this reaction is still controversial. The *ab initio* molecular orbital calculations reported here predict that the main reaction pathway includes the formation of a three-electron-bonded adduct followed by the elimination of the hydroxide anion, giving the sulfinyl radical as the reaction product. The alternative reaction pathway consisting of hydrogen atom transfer from the thiol to the protonated superoxide radical involves a reaction energy barrier that is significantly higher. The difference between the two reaction energy barriers is clearly beyond the expected computational uncertainty. The systematic scanning of the potential energy surface reveals no other competitive reaction pathways. The present results provide a useful basis for the interpretation of the complex experimental data related to thiol oxidation by superoxide radical in a biological environment.

Introduction

The superoxide radical anion ($O_2^{\bullet -}$) is one of the most important reactive oxygen species (ROS) responsible for oxidative stress in bio-organisms. It is generated as a byproduct of the mitochondrial respiratory chain.[1] A high percentage of this weakly active radical will undergo rapid disproportionation to hydrogen peroxide and oxygen in a reaction catalyzed by the manganese-containing superoxide dismutase (Mn−SOD).[2] Disproportionation may also occur spontaneously in the presence of the perhydroxyl radical that is the protonated superoxide radical ($HO_2^{\bullet}$):

$$O_2^{\bullet -} + HO_2^{\bullet} + H^+ \rightarrow H_2O_2 + O_2 \quad (1)$$

The remaining superoxide radical anion is supposed to be scavenged by the natural antioxidant glutathione (GSH), which is present in living cells at concentrations as high as 10 mM.

The mechanism of this later reaction is still controversial: According to some authors[3−5] the superoxide radical reacts with thiols (RSH) by hydrogen atom abstraction giving the thiyl radical and hydrogen peroxide (channel a):

$$O_2^{\bullet -} + RSH + H^+ \rightarrow RS^{\bullet} + H_2O_2 \quad (2)$$

Other authors[6−8] consider that the first step of the reaction is the formation of a three-electron-bonded radical, which breaks down into a sulfinyl radical and a hydroxide anion (channel b):

$$O_2^{\bullet -} + RSH \rightarrow RS(OOH)^{\bullet -} \quad (3)$$

$$RS(OOH)^{\bullet -} \rightarrow RSO^{\bullet} + HO^- \quad (4)$$

In both reaction schemes it is assumed that the intermediate radical $RS^{\bullet}$ or $RSO^{\bullet}$ will further interact with thiolate to give rise to the final disulfide RSSR. Interestingly, the reported reaction rate constants show peculiar discrepancies: they range between 10 and 10^3 dm^3 mol^{-1} s^{-1} (ref 4−8) although values as high as 10^5 dm^3 mol^{-1} s^{-1} have also been reported.[3] The present situation may be explained by the specific complexity of the experimental conditions required for measuring this reaction rate constant: other oxidant species, such as H_2O_2 and $OH^{\bullet}$, are present and the effects of their competition with $O_2^{\bullet -}$ are difficult to take into account.

The importance of the three-electron-bonded adducts in the oxidative processes involving radicals has already been emphasized.[9−12] Consequently, the interest in studying the binding and the properties of such kind of adducts is increasing. The theoretical analysis based on *ab initio* molecular orbital calculations proved to be very efficient for this purpose.[13−16] Indeed, it is known that such calculations when performed at a high level of theory are often able to predict reaction energy barriers with chemical accuracy. This has been recently proved for the particular case of thiol oxidation by H_2O_2 and $OH^{\bullet}$ in aqueous solutions.[17,18] The contribution of an *ab initio* molecular orbital study to clarify the mechanism of thiol oxidation by the superoxide radical is thus expected to be significant.

In the present paper the interaction between thiol and the superoxide radical in its anionic ($O_2^{\bullet -}$) and protonated ($HO_2^{\bullet}$) forms has been analyzed in a systematic manner and at a high level of the *ab initio* molecular orbital theory. The reaction pathways are determined and the reaction energy barriers are calculated, both *in vacuo* and in aqueous solution. The theoretical predictions are compared to the experimental data and conclusions are drawn concerning the prevalence of channel a or channel b in thiol oxidation by the superoxide radical.

Computational Method

All calculations were performed with the GAUSSIAN 03 program package[19] using methanethiol (CH_3SH) as the model thiol.

To locate the stationary points (transition states and other reaction intermediates), the potential energy surface (PES) of the reactant system was separately scanned with respect to the significant geometry parameters that are expected to change during the reaction: the S−O, H_S (H on sulfur)−O, S−H_S, and O−O distances. A point on a scan curve corresponds to a

* Corresponding author. E-mail: mironel.enescu@univ-fcomte.fr. Fax: (+33) 3 81 66 65 22. Tel: (+33) 3 81 66 65 21.

10.1021/jp0731102 CCC: $37.00
Published on Web 11/29/2007

geometry optimized with respect to all parameters, except for the scan coordinate. The scans were performed using the density functional theory (DFT) method with the B3LYP[20] hybrid functional and the 6-311+G(d,p) basis set. Once identified on the scan trajectories, the molecular intermediates were further optimized without constraints. A first optimization was performed using the UB3LYP/6-311+G(d,p) level of theory. Frequency calculations confirmed that each of the transition states identified possess only one imaginary frequency. Intrinsic reaction coordinate (IRC)[21] calculations were also performed to check that the reactants and products are directly connected by the transition states previously identified.

With respect to the geometry optimization of the three-electron-bonded systems, it has already been emphasized that the DFT methods systematically fail in predicting accurate structures.[14,15] In the present study we have reoptimized the stationary structures using the Møller−Plesset many-body perturbation theory to second- or fourth-order in their spin-unrestricted form (UMP2/6-311+G(d,p) and UMP4/6-311+G-(d,p), respectively). Significant differences between DFT, UMP2, and UMP4 optimized structures were found in the case of the transition state TS2 (see below). We further checked the convergence of the TS2 optimized structure with respect to the level of theory used in the *ab initio* calculation by performing a QCISD/6-311+G(d,p) optimization. The differences with respect to the UMP4/6-311+G(d,p) optimized geometry were still non-negligible. We concluded that for accurate structure calculation, a theory level equivalent to or higher than QCISD/6-311+G(d,p) is required. Interestingly, the integrated molecular orbital + molecular orbital (IMOMO) method[22] was found to give optimized structures very close to that given by QCISD/6-311+G(d,p) (in the case of TS2 the interatomic distance deviations were less than 0.02 Å). In IMOMO calculations, the model system, treated at the QCISD/6-311+G(d,p) level of theory, was SH_2+ $O_2^{\bullet-}$ and the real system, treated at the UMP2/6-311+G(d,p) level of theory, was CH_3SH+ $O_2^{\bullet-}$. Finally, the IMOMO method was preferred because it is significantly faster, thus allowing additional frequency calculations to be performed as required in the application of the variational transition state theory. Hence, all the optimized geometries reported here were calculated by using the IMOMO method.

The optimized geometries were further used for single point energy calculations at a higher level of theory.

The standard gas-phase Gibbs free energy (G_g) of a molecular state M was calculated as follows:

$$G_g(M) = E_{p,g}(M) + \Delta G_{c,g}(M) \quad (5)$$

Here $E_{p,g}(M)$ is the gas-phase molar potential energy and $\Delta G_{c,g}(M)$ is the molar Gibbs free energy correction calculated at 298 K and 1 atm. The zero-point corrected energy ($E_{0,g}$) and the standard enthalpy (H_g) were obtained in a similar manner by adding the zero-point energy correction or the enthalpy correction to the molar potential energy. The thermal corrections were obtained by performing frequency calculations using the IMOMO method, as described above. The potential energy $E_{p,g}(M)$ was calculated using the quadratic configuration interaction, including simple and double substitutions with a triplet contribution to energy added (QCISD(T))[23] and the 6-311+G(2df,-2pd) basis set.

The standard Gibbs free energy in aqueous solution (G_{aq}) was calculated using the following formula:

$$G_{aq}(M) = G_g(M) + G_{solv}(M) \quad (6)$$

TABLE 1: Relative[a] Gibbs Free Energy (at 298 K, in kJ mol^{-1}) in the Gas Phase (ΔG_g) and Aqueous Solution (ΔG_{aq}) of Some Possible Products of the Methanethiol Oxidation by the Superoxide Radical Anion Calculated at the QCISD(T)/6-311+G(2df,2pd)//IMOMO[b] Level of Theory[c]

product	ΔG_g	ΔG_{aq}
$CH_3SO^{\bullet} + HO^-$	−123.9	−170.5
$CH_3SO^- + HO^{\bullet}$	−60.0	−52.5
$CH_3S^- + HO_2^{\bullet}$	13.4	32.2
$CH_3S^{\bullet} + HO_2^-$	85.4	68.2

[a] Reference state: free reactants [b] QCISD/6-311+G(d,p) for model and UMP2/6-311+G(d,p) for the real system. [c] The solvation energy was calculated with the IPCM method.

where G_{solv} is the solvation free energy. The solvation free energy was obtained with the isodensity version of the polarizable continuum model (IPCM).[24] In this version of the polarizable continuum model, the atomic cavities of the solute system are not predefined but are determined on the basis of the electronic isodensity surface calculations. This method is *a priori* more appropriate for describing the solvation of molecular systems with peculiar electronic distribution, such as transition states and three-electron-bonded complexes. The solvation energy was calculated at the UMP2/6-311+G(d,p) level of theory as the difference between the energy of the solvated structure and that of the gas-phase structure. To calculate the free energies of solvation, all structures were reoptimized in the solvent. Because in the GAUSSIAN 03 program package gradient calculations with the IPCM method are not implemented yet, the solvent optimizations were performed using the IEF-PCM version[25] of the polarizable continuum model.

The nature of the intermediates identified along the reaction trajectory was also investigated by performing natural population analysis (NPA)[26] giving spin density distribution and partial atomic charges.

Results

Interaction of Methanethiol with $O_2^{\bullet-}$. The anionic form $O_2^{\bullet-}$ of the superoxide radical is largely dominant at neutral pH because the pK_a of the $HO_2^{\bullet}/O_2^{\bullet-}$ couple is 4.8.[27] Several product couples could be, in principle, produced by the interaction of $O_2^{\bullet-}$ with CH_3SH: $CH_3SO^{\bullet} + HO^-$ (FP1), $CH_3SO^- + HO^{\bullet}$ (FP2), $CH_3S^- + HO_2^{\bullet}$ (FP3), and $CH_3S^{\bullet} + HO_2^-$ (FP4). Among them, those having Gibbs free energy values higher than that of the free reactants (FR) are not stable reaction products. The relative Gibbs free energies of products FP1 to FP4 are listed in Table 1. These values were calculated in aqueous solution by taking the free reactants as the reference state. Interestingly, only the product couples FP1 and FP2 are more stable than FR in aqueous solution. On the other hand, the relative Gibbs free energy of FP1 is considerably lower than that of FP2. Hence, finding a reaction pathway connecting FR and FP1 will prove that the couple sulfinyl radical and hydroxide anion are by far the most important product of thiol oxidation by $O_2^{\bullet-}$.

PES scans with respect to H_S−O or O−S distances performed with the DFT method (not shown) indicate that, at intermediate distances, the two reactants adopt a relative configuration favorable for H bond formation between H_S and O. When the H_S−O distance decreases below 1.6 Å, a proton transfer from S to O occurs. This proton transfer has no energy barrier *in vacuo* and a negligible one in aqueous solution. The reactant complex (RC) formed upon proton transfer is stabilized by H bonding. Its structure reoptimized with the IMOMO method is shown in Figure 1. The NPA analysis clearly indicates that the

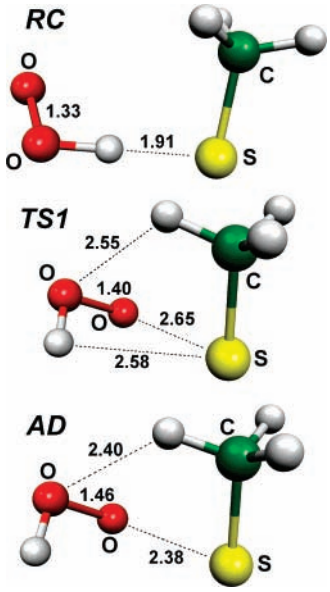

Figure 1. CH_3SH oxidation by $O_2^{\bullet-}$: images of the reactant complex RC, transition state TS1, and three-electron-bonded adduct AD. Atom distances are given in Å. Geometries optimized *in vacuo* with the IMOMO method combining QCISD/6-311+G(d,p) and UMP2/6-311+G(d,p) levels of theory for the model and the real system, respectively.

spin density on the S atom (that is the difference between the α spin and β spin electronic populations) is negligible and the corresponding natural charge is about −0.70 e. Hence, RC is a complex between CH_3S^- and $HO_2^{\bullet}$ and may be considered as the precursor of FP3. On the other hand, an electronic state precursor of FP4 could be in principle generated from RC by electron transfer from CH_3S^- to $HO_2^{\bullet}$. Despite the systematic PES scans performed *in vacuo* with respect to the O−O or S−H distances we failed to locate a transition state for this electron transfer. This result suggests that, at least *in vacuo*, the precursor of FP4 is an electronic excited state whose PES does not cross the PES of the electronic ground state. Instead, the adiabatic coupling of the two energy surfaces could occur in aqueous solution where a new coordinate, the solvent reorganization, participates in the system evolution. However, the point is not very important for the present analysis because even in aqueous solution FP4 is not a stable reaction product (see Table 1).

The only interesting evolution of RC remains that leading to the formation of a S−O adduct. The corresponding transition state (TS1) located by scanning PES with respect to the S−O distance and reoptimized with the IMOMO method is shown in Figure 1. The connection between the RC and TS1 was checked at the DFT level of theory. The backward IRC calculation (Figure 2) started from TS1 led to a $CH_3S^-\cdots HO_2^{\bullet}$ complex similar to RC but not identical. The passage between the two complexes consists of a simple relative reorientation of CH_3S^- and $HO_2^{\bullet}$ with practically no energy barrier. On the other hand, the forward IRC calculation led to a S−O adduct we denoted AD (IMOMO structure given in Figure 1). The NPA analysis on AD indicates that the unpaired spin is completely located on S and O_S atoms and the sum of the natural charges of these atoms is −0.77. We conclude that AD is a three-electron-bonded adduct. Besides the tree electron S−O bond, AD is also stabilized by two H-bonds formed between H_O and S and O_H and H_C (H from methyl group), respectively (Figure 1).

The transition from RC to AD affects also the O−O distance: it changes from 1.33 Å, which is the O−O distance

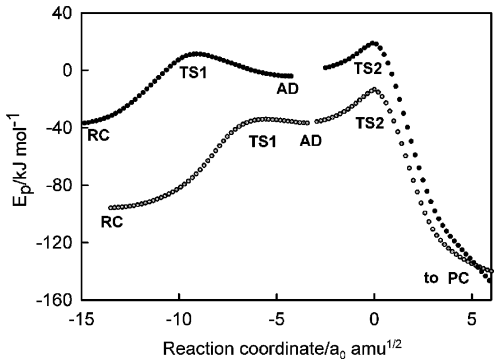

Figure 2. Gas-phase (open circles) and aqueous solution (solid circles) reaction trajectories for the CH_3SH oxidation by $O_2^{\bullet-}$ (channel b) calculated at the UB3LYP/6-311+G(d,p) level of theory. A trajectory was obtained by joining the IRC curves for the transition states TS1 and TS2.

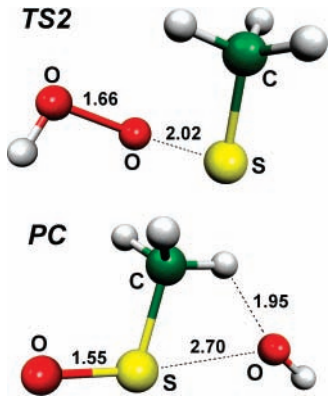

Figure 3. CH_3SH oxidation by $O_2^{\bullet-}$: images of the transition state TS2 and product complex PC. Atom distances are given in Å. Geometries optimized *in vacuo* with the IMOMO method combining QCISD/6-311+G(d,p) and UMP2/6-311+G(d,p) levels of theory for the model and the real system, respectively.

for optimized $HO_2^{\bullet}$, to 1.46 Å, which is identical to the O−O distance in the optimized hydrogen peroxide. Consequently, the energy barrier for breaking the O−O bond is significantly lowered and the related transition state, TS2 (IMOMO reoptimized structure given in Figure 3), becomes accessible. The IRC calculations (Figure 2) show that TS2 is directly connected to AD, on one side of the reaction pathway, and to a H-bonded complex we denoted PC, on the other side. According to the NPA analysis, the negative charge in the PC complex is located on O_H (−0.98) and the unpaired spin is shared between S and O_S. Hence PC (IMOMO reoptimized structure in Figure 3) may be represented as $RSO^{\bullet}\cdots HO^-$ and is the precursor of the $RSO^{\bullet} + HO^-$ product. On the other hand, an electron transfer from HO^- to $RSO^{\bullet}$ would lead to the precursor of the $RSO^- + HO^{\bullet}$ product. However, this alternative reaction pathway is not very interesting because the latter product is significantly less stable with respect to the $RSO^{\bullet} + HO^-$ couple.

The geometries in Figures 1 and 3 were further used to calculate zero point corrected energies, enthalpies, and Gibbs free energies for the stationary states on the reaction trajectory, as described in the preceding section. The relative values of these parameters calculated by tacking FR as reference state are given in Table 2. It appears that the gas-phase zero point corrected energies of TS1, AD, and TS2 are all slightly inferior to that of FR. This is also the case for the gas-phase enthalpies. However, the gas-phase Gibbs free energies of these bounded states are all positive due to a smaller contribution of the translation entropy as compared to FR. The maximum G_g value

TABLE 2: Relative[a] Thermodynamic Parameters (at 298 K, in kJ mol^{-1}) for the Molecular Stationary Structures Involved in the Oxidation of Methanethiol by the Superoxide Radical Anion Calculated at the QCISD(T)/6-311+G(2df,2pd)//IMOMO[b] Level of Theory[c]

	$\Delta E_{0,g}$[d]	ΔH_g[d]	ΔG_g[d]	ΔG_{aq}[d]
RC	−99.7	−98.7	−72.6	−2.2
TS1	−12.7	−13.4	22.1	75.3
AD	−15.9	−15.7	19.1	67.1
TS2	−10.1	−10.5	25.4	69.7
PC	−221.0	−221.4	−184.4	−147.6

[a] Reference state: free reactants (FR). [b] QCISD/6-311+G(d,p) for model and UMP2/6-311+G(d,p) for the real system. [c] The solvation energy was calculated with the IPCM method. [d] $\Delta E_{0,g}$ is the zero point corrected energy, ΔH_g is the gas-phase enthalpy, ΔG_g is the gas-phase Gibbs free energy, and ΔG_{aq} is the aqueous solution Gibbs free energy.

corresponds to the TS2 state. In aqueous solution the theoretical reaction energy barrier rises significantly because FR is more soluble as compared to the bounded states of RC, TS1, TS2, AD, and PC. The ΔG_{aq} values of the molecular intermediates TS1, AD, and TS2 are very close to each other, and the highest value of 75.3 kJ mol^{-1} is reached in TS1. Given the strong solvation effect upon the Gibbs free energy, the choice of the computational method for solvation energy calculation is expected to have an important impact on the final result. Fortunately, the reaction energy barrier depends on the relative solvation energy, which is a more stable parameter compared to the absolute solvation energy. A comparison between relative solvation energies calculated for the same molecular intermediate using two solvation methods, IPCM and IEF-PCM respectively, showed differences up to 10 kJ mol^{-1}. For the reason explained in the Computational Method section, in the present work the IPCM values were systematically preferred.

Strictly speaking, the exact location of the effective transition state along the reaction pathway would require the application of the variational transition state theory[28] because the PES are rather flat between TS1 and TS2. In the canonical formulation of this theory (CVT), the effective transition state corresponds to the point on the minimum energy path (MEP) having the maximum Gibbs free energy. In the present work we have determined the MEP around TS1 and TS2 by performing IRC calculations with a step of 0.05 a_0 amu$^{1/2}$ (a_0 being the Bohr radius) using the IMOMO method (QCISD+UMP2). The Gibbs free energy in aqueous solution was then evaluated for every point on the MEP curve using the method described in the preceding section. For both TS1 and TS2, the CVT correction induces a slight displacement of the transition state but the changes in the energy barriers are smaller than 0.5 kJ mol^{-1} (Figures 4 and 5).

We conclude that the limiting step along the reaction pathway is the transition across TS1. Because the relative Gibbs free energy of the RC complex is negative, its formation is diffusion limited and the effective reaction energy barrier is the relative Gibbs free energy of the TS1 state.

With respect to the quantum tunneling effects, they need to be considered only for the RC → AD transition because the AD → PC transition is predicted to be diffusion limited because the energy barrier is only 2 kJ mol^{-1}. The tunneling coefficient for the RC → AD transition calculated in the gas phase using the truncated parabola model of Auerbach and Fermann[28] was 1.13. A precise evaluation in aqueous solution is not possible because we cannot separate the zero-point-corrected energy contribution to the PCM solvation Gibbs free energy. Assuming that the whole difference between the solvation Gibbs free

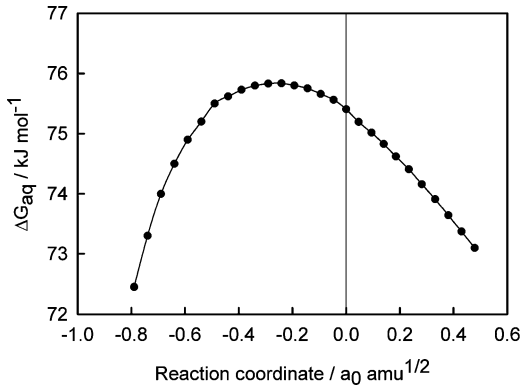

Figure 4. Gibbs free energy curve in aqueous solution calculated near the TS1 transition state as follows: the MEP curve was determined by the IMOMO method, then the Gibbs free energy was evaluated at every point on the MEM at the QCISD(T)/6-311+G(2df,2pd)//IMOMO level of theory. Here IMOMO means QCISD/6-311+G(d,p) + UMP2/6-311+G(d,p). The solvation energy was calculated with the IPCM method.

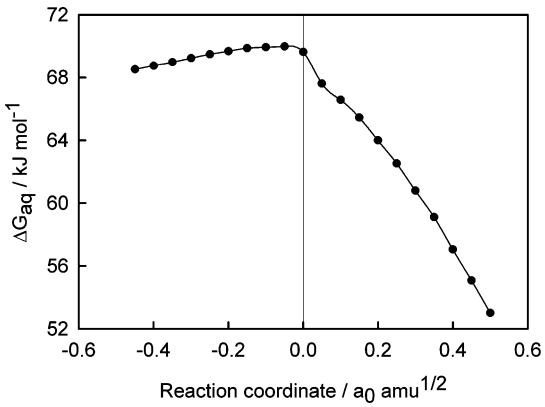

Figure 5. Gibbs free energy curve in aqueous solution calculated near the TS2 transition state as follows: the MEP curve was determined by the IMOMO method; then the Gibbs free energy was evaluated at every point on the MEM at the QCISD(T)/6-311+G(2df,2pd)//IMOMO level of theory. Here IMOMO means QCISD/6-311+G(d,p) + UMP2/6-311+G(d,p). The solvation energy was calculated with the IPCM method.

energy of AD and RC comes from the zero-point-corrected energy, the zero-point-corrected energy barrier will decrease from 87 to about 70 kJ mol^{-1}. This decrease has little effect on the tunneling coefficient.

Interaction of Methanethiol with $HO_2^{\bullet}$. At biological pH the concentration of the perhydroxyl radical is a hundred times smaller than that of $O_2^{\bullet -}$. However, this alternative form of the superoxide radical could play a role in the thiol oxidation if a reaction pathway specific to it, with a low enough energy barrier, was possible. A PES scan with respect to the O−S_H distance performed at the DFT level of theory (Figure 6) reveals the presence of a transition state (TS1′) connecting a H-bound reactant complex (RC′) to a product complex PC1′. The three structures reoptimized with the IMOMO method are given in Figure 7. The O−O distance in PC1′ is almost identical to that characteristic for free hydrogen peroxide (H_2O_2) and the NPA analysis indicates that the unpaired spin is exclusively located on the sulfur. PC1′ is thus the precursor of the product couple $CH_3S^{\bullet}$ + H_2O_2 (FP1′). The chemical transformation related to the transition state TS1′ is a H atom abstraction from CH_3SH to $HO_2^{\bullet}$ (channel a in the preceding notation). The thermodynamic parameters of the free reactants (FR′), free products (FP1′), and intermediate states are given in Table 3. According to these data, the Gibbs free energy of FP1′ is slightly inferior

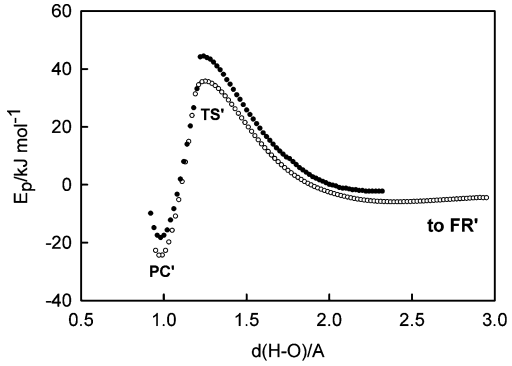

Figure 6. Gas-phase (open circles) and aqueous solution (solid circles) reaction trajectories for CH_3SH oxidation by $HO_2^{\bullet}$ (channel a). The curves were obtained by scanning the PES with respect to the H_S-O distance at the UB3LYP/6-311+G(d,p) level of theory.

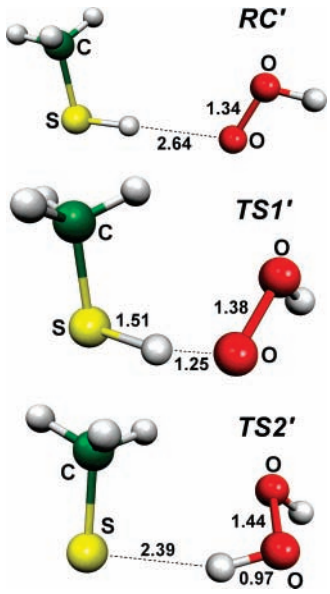

Figure 7. CH_3SH oxidation by $HO_2^{\bullet}$: images of reactant complex RC′, transition state TS1′ and product complex PC1′. Atom distances are given in Å. Geometries optimized *in vacuo* with the IMOMO method combining QCISD/6-311+G(d,p) and UMP2/6-311+G(d,p) levels of theory for the model and the real system, respectively.

TABLE 3: Relative[a] Thermodynamic Parameters (at 298 K in kJ mol^{-1}) for the Molecular Stationary Structures and Free Products Involved in the Methanethiol Oxidation by the Perhydroxyl Radical Calculated at the QCISD(T)/6-311+G(2df,2pd)//IMOMO[b] Level of Theory[c]

	$\Delta E_{0,g}$[d]	ΔH_g[d]	ΔG_g[d]	ΔG_{aq}[d]
RC′	−7.2	−3.2	25.3	38.5
TS1′	47.1	42.3	87.2	89.9
PC1′	−23.0	−22.6	10.0	12.1
TS2′	108.6	105.0	151.3	111.6
PC2′	−294.7	−292.0	−265.6	−274.9
$CH_3S^{\bullet} + H_2O_2$	−6.7	−7.3	−5.4	−11.3
$CH_3SO^{\bullet} + H_2O$	−263.2	−262.1	−257.4	−278.7

[a] Reference state: free reactants (FR′). [b] QCISD/6-311+G(d,p) for model and UMP2/6-311+G(d,p) for the real system. [c] The solvation energy was calculated with the IPCM method. [d] $\Delta E_{0,g}$ is the zero point corrected energy, ΔH_g is the gas-phase enthalpy, ΔG_g is the gas-phase Gibbs free energy, and ΔG_{aq} is the aqueous solution Gibbs free energy.

to that of FR′. On the other hand, the relative Gibbs free energy of TS1′ representing the reaction energy barrier is 89.9 kJ mol^{-1}. This value is calculated by tacking FR′ as the reference state. To compare this value to the energy barrier for channel b, one should add 49 kJ mol^{-1}, which corresponds to the Gibbs free energy difference between FR′ and FR. This difference was calculated using the experimental pK_a value[27] of the $HO_2^{\bullet}/O_2^{\bullet-}$ couple. The resulting energy barrier is significantly higher than that involved in channel b, indicating that H abstraction is a minor reaction channel.

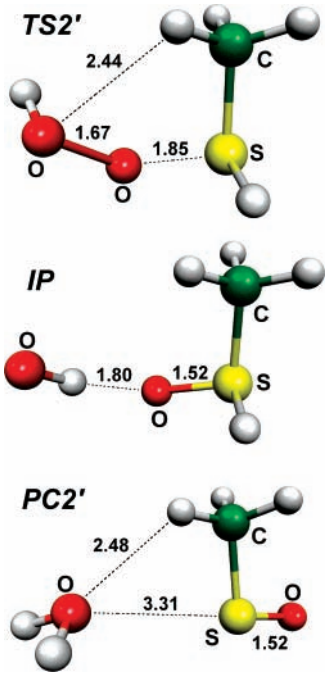

Figure 8. CH_3SH oxidation by $HO_2^{\bullet}$: images of the transition state TS2′, intermediate product IP and the product complex PC2′. Atom distances are given in Å. Geometries optimized *in vacuo* with the IMOMO method combining QCISD/6-311+G(d,p) and UMP2/6-311+G(d,p) levels of theory for the model and the real system, respectively.

For this reactant couple an alternative reaction pathway is also possible, involving an O−S interaction that finally induces the breaking of the O−O bond. Indeed, the PES scan with respect to the O−S distance allowed us to locate the corresponding transition state TS2′ (IMOMO reoptimized structure given in Figure 8). The backward IRC calculation (not shown) leads to the reactant couple $CH_3SH + HO_2^{\bullet}$, and the forward calculation leads to an intermediate product IP. Spin density analysis shows that IP is a complex formed between the hydroxyl radical $OH^{\bullet}$ and the hydrogen methyl sulfoxide, CH_3SHO, which is a rather unstable molecular structure. This intermediate decays to the more stable product complex, PC2′ (IMOMO reoptimized structure in Figure 8), following a reaction pathway with negligible energy barrier. According to the NPA analysis, PC2′ is a complex of sulfinyl radical $CH_3SO^{\bullet}$ with a water molecule. Hence this alternative reaction pathway represents, for the case of the protonated superoxide radical, a reaction channel equivalent to channel b. However, the reaction energy barrier in this present case is very high, about 111.6 kJ mol^{-1} calculated with respect to the FR′ state (Table 3). The effective energy barrier, calculated with respect to FR, is 160.1 kJ mol^{-1}. Consequently, the formation of sulfinyl radical by this reaction channel is very unlikely.

Discussion

The present theoretical analysis predicts that the formation of the sulfinyl radical is the dominant first step in thiol oxidation by the superoxide radical. The reaction mechanism involves the formation of a three-electron-bonded adduct followed by the

elimination of the hydroxide anion (channel b). Interestingly, a similar reaction mechanism involving two transition states connected by a three-electron-bonded adduct was also predicted for the CO oxidation by the perhydroxyl radical to form CO_2 and $HO^{\bullet}$.[9] With respect to the three-electron-bonded adduct AD reported here, one notes it is isoelectronic with the biological important disulfide anion $[R_1S \therefore SR_2]^-$.[29] However, although the latter is stable enough to be detected in pulse radiolysis experiments, AD is predicted to be very unstable because the energy barrier for its transition to the product complex PC is only 2.6 kJ mol^{-1}.

When the superoxide radical in its protonated form is considered, a H-atom transfer process is also possible (channel a), the related energy barrier is about 64 kJ mol^{-1} higher with respect to that of channel b. This difference is definitely beyond the uncertainty expected for the computational method employed here. This result strongly supports those experimental studies that conclude the prominence of sulfinyl radical formation upon thiol oxidation by the superoxide radical.

The validation of the reaction mechanism proposed here requires careful comparison with experimental data. A first question concerns the relevance of methanethiol as a model for the more complex thiols, such as acetylcysteine, glutathione, or dithiothreitol, for which experimental reaction rate constants are available. These reported values vary greatly, but it is not clear whether the thiol type plays a role in this dispersion. For instance, reaction rate constants of 35 mol^{-1} dm^3 s^{-1} for dithiothreitol,[6] 24 mol^{-1} dm^3 s^{-1} for glutathione,[30] and 68 mol^{-1} dm^3 s^{-1} for *N*-acetylcysteine[7] have been reported. Given the fact that for glutathione the reaction rate constants as high as 10^3 and even 10^5 mol^{-1} dm^3 s^{-1} (ref 3) have also been proposed, it appears that the thiols diversity is not the main reason for these discrepancies. Moreover, in the case of a rather similar reaction, that of thiol oxidation by hydrogen peroxide, the reaction rate constants reported for various thiols (cysteine, cysteamine, GSH, penicillamine, dithiothreitol) are remarkably constant with values varying between 18 and 26 mol^{-1} dm^3 s^{-1}.[8] A recent theoretical analysis on cysteine oxidation by hydrogen peroxide showed that including interaction of the side atoms has some effect on the calculated reaction energy barrier.[31] However, this effect was found to be significant (a deviation of about 15 kJ mol^{-1} with respect to the reaction energy barrier calculated for methanethiol) only *in vacuo*, and the solvent is predicted to strongly attenuate it. It is then reasonable to assume that the energy barrier calculated for the oxidation of methanethiol by the superoxide radical is relevant at least in terms of order of magnitude for the case of more complex thiols.

A direct comparison of our calculated reaction energy barrier of 75.3 kJ mol^{-1} with the experimental data is not possible because, to the best of our knowledge, no experimental energy barrier has yet been reported for this reaction. However, a satisfactory estimation of the experimental energy barrier can be obtained on the basis of the experimental reaction rate constant and its TST expression:[17]

$$k = (k_B T/h) c_0 \exp[-\Delta G_{aq}(TS)/RT] \quad (7)$$

Here k_B is the Boltzmann constant, h is the Planck constant, R is the gas constant, T is the temperature, and c_0 is the standard molar concentration in solution (1 mol dm^{-3}). Assuming a k value of 35 mol^{-1} dm^3 s^{-1} as reported for dithiothreitol,[6] eq 7 gives an estimated reaction energy barrier of about 65 kJ mol^{-1} at $T = 298$ K. The deviation of the theoretical value with respect to this estimated experimental value is about 10 kJ mol^{-1}. Obviously, part of this deviation is related to the inherent computational difficulties in treating the three-electron-bonded anions.[15] For stable three-electron-bonded anions (F_2^-, Cl_2^-, I_2^-, ClI^-, and BrI^-) the CCSD(T) level of theory (that is approximately equivalent to the QCISD(T) level) was found to give dissociation energies that were in good agreement with the experimental data. The mean deviation between the theoretical and the experimental dissociation energy was found to be about +4 kJ mol^{-1}.[14] However, the error is expected to be higher in the case of the unstable anions,[15] thus affecting the Gibbs free energy values calculated in the present work for the TS1, AD ,and TS2 states. The calculated solvation energy differences could also contribute in some manner to the overall error affecting our results. Finally, the agreement between the calculated energy barrier and those experimental reaction rate constants reported in the interval between 10 and 100 mol^{-1} dm^3 s^{-1} can be judged as satisfactory. On the other hand, an experimental reaction rate constant of the order of 10^5 mol^{-1} dm^3 s^{-1} would imply a theoretical overestimation of the reaction energy barrier of about 34 kJ mol^{-1}, which seems very unlikely.

Conclusion

The interaction of the superoxide radical (in both anionic and protonated form) with the model system methanethiol has been investigated at a high level of *ab initio* molecular orbital theory. Gibbs free energy calculations indicate that, in aqueous solution, among the possible reaction products the most stable is the $CH_3SO^{\bullet} + HO^-$ couple. Systematic PES scan and IRC calculations allowed us to identify the reaction pathway connecting the free reactants and the precursor of this product. The reaction mechanism consists of the formation of a three-electron-bonded anion followed by the elimination of the hydroxide anion.

The present results strongly support the formation of the sulfinyl radical as the first step in thiol oxidation by the superoxide radical. The analysis reported here could be very useful in interpreting the experimental data related to thiol oxidation in a biological environment.

Supporting Information Available: Cartesian coordinates for the transition states TS1, TS2, TS1′, and TS2′ and for the adduct AD as well as the corresponding Gaussian 03 input files used in geometry optimization; Gaussian 03 input file for single point energy calculation on the transition state TS1 at the QCISD(T)/6-311+G(2df,2pd) level of theory; Gaussian 03 input file for IPCM solvation energy calculation of TS1; detailed thermodynamic parameters for all the molecular structures involved in the oxidation of methanethiol by the superoxide radical. This material is available free of charge via Internet at http://pubs.acs.org.

References and Notes

(1) Turrens, J. F.; Boveris, A. *Biochem. J.* **1980**, *191*, 421−427.
(2) Cadenas, E.; Davies, K. *J. Free Rad. Biol., Med.* **2000**, *29*, 222−230.
(3) Dikalov, S.; Khramtsov, V.; Zimmer, G. *Arch. Biochem. Biophys.* **1995**, *326*, 207−218.
(4) Jones, C. M.; Lawrence, A.; Wartman, P.; Burkitt, M. J. *Biochem. Soc. Trans.* **2003**, *31*, 1337−1339.
(5) Feroci, G.; Fini, A. *Inorg. Chim. Acta* **2007**, *360*, 1023−1031.
(6) Zhang, N.; Schuchmann, H.-P.; von Sonntag, C. *J. Phys. Chem.* **1991**, *95*, 4718−4722.
(7) Benrahmoune, M.; Thérond, P.; Abedinzadeh, Z. *Free Rad. Biol. Med.* **2000**, *29*, 775−782.
(8) Winterbourn, C. C.; Metodiewa, D. *Free Rad. Biol. Med.* **1999**, *27*, 322−328.
(9) Allen, T. L.; Fink, W. H.; Volman, D. H. *J. Phys. Chem.* **1996**, *100*, 5299−5302.
(10) Rauk, A.; Armstrong, D. A.; Fairlie, D. P. *J. Am. Chem. Soc.* **2000**, *122*, 9761−9767.

(11) Schöneich, C.; Pogocki, D.; Wisniowski, P.; Hug, G. L.; Bobrowski, K. *J. Am. Chem. Soc.* **2000**, *122*, 10224−10225.

(12) Mohan, H.; Mittal, J. P. *J. Phys. Chem. A* **2002**, *106*, 6574−6580.

(13) Humbel, S.; Côte, I.; Hoffman, N.; Bouquant, J. *J. Am. Chem. Soc.* **1999**, *121*, 5507−5512.

(14) Chermette, H. *J. Chem. Phys*. **2001**, *115*, 11068−11078.

(15) Braïda, B.; Thogersen, L.; Wu, W.; Hiberty, P. *J. Am. Chem. Soc*. **2002**, *124*, 11781−11790.

(16) Maity, D. *J. Am. Chem. Soc*. **2002**, *124*, 8321−8328.

(17) Cardey, B.; Enescu, M. *ChemPhysChem.* **2005**, *6*, 1175−1180.

(18) Enescu, M.; Cardey, B. *ChemPhysChem.* **2006**, *4*, 912−919.

(19) Frisch, M. J.; et al. *Gaussian 03*, revision B.04; Gaussian, Inc.: Pittsburgh, PA, 2003.

(20) Becke, A. D. *J. Chem. Phys.* **1993**, *98*, 5648−5652.

(21) Gonzales, C.; Schlegel, H. B. *J. Phys. Chem*. **1990**, *94*, 5523−5527.

(22) Svensson, M.; Humbel, S.; Morokuma, K. *J. Chem. Phys*. **1996**, *105*, 3654−3661.

(23) Pople, J. A.; Head-Gordon, M.; Raghavachari, K. *J. Chem. Phys*. **1987**, *87*, 5968−5975.

(24) Foresman, J. B.; Keith, T. A.; Wilberg, K. B.; Snoonian, J.; Frish, M. J. *J. Phys. Chem.* **1996**, *100*, 16098−16104.

(25) Cossi, M.; Scalmani, G.; Rega, N.; Barone, V. *J. Chem. Phys*. **2002**, *117*, 43−54.

(26) Reed, A. E.; Weinstock, R. B.; Weinhold, F. *J. Chem. Phys*. **1985**, *83*, 735−746.

(27) Bieliski, B. H. J.; Cabelli, D. E.; Arudi, R. L.; Ross, A. B. *J. Phys. Chem. Ref. Data* **1985**, *14*, 1041−1100.

(28) Truhlar, D. G.; Garett, B. C. *Acc. Chem. Res*. **1980**, *13*, 440−448.

(29) Mezyk, S. P. *Chem. Phys. Lett*. **1995**, *335*, 89−93.

(30) Winterbourn, C. C.; Metodiewa, D. *Arch. Biochem. Biophys*. **1994**, *314*, 284−290.

(31) Cardey, B.; Enescu, M. *J. Phys. Chem*. *A* **2007**, *111*, 673−678.